J. Fluid Mech. (1988), *vol.* 192, *pp.* 75–96
Printed in Great Britain

Similarity solutions for two-dimensional steady laminar gravity currents

By P. W. M. BRIGHTON
Safety and Reliability Directorate, UKAEA, Wigshaw Lane, Culcheth, Warrington WA3 4NE, UK

(Received 29 December 1986 and in revised form 8 July 1987)

Similarity solutions have been found for steady two-dimensional laminar flow in which dense fluid is emitted upwards from a horizontal plane into a laminar shear flow or into a uniform flow. The solutions also apply to a light fluid released at an upper horizontal surface. The Navier–Stokes equations and the diffusion–advection equation are simplified by making the Boussinesq approximation and the boundary-layer approximation, which here also implies that pressure is hydrostatic.

For an oncoming linear shear flow representing flow near a solid surface, a similarity solution is obtained with depth proportional to $x^{\frac{1}{3}}$ where x is the horizontal coordinate. Horizontal velocity and concentration of dense fluid both increase as $x^{\frac{1}{3}}$, so that the solution represents fluid propagating upstream along the surface, and diffusing vertically to be swept downstream again. Numerical solutions for vertical profiles of velocity and concentration are presented for a Schmidt or Prandtl number σ between 0.71 and infinity. Two alternative sets of boundary conditions are possible. In one set, the pressure above the boundary layer is unchanged but the velocity profile is displaced upwards. In the second, this displacement is forced to be zero with the result that a pressure gradient is generated in the outer flow. These two boundary conditions are known to apply to disturbances in a laminar boundary-layer on horizontal lengthscales respectively greater or smaller than the triple-deck scale.

With a uniform velocity upstream and a stress-free boundary, representing flow at a free surface, similarity solutions exist only for a plume growing downstream from the source of a buoyancy flux B, with depth increasing as $x^{\frac{1}{2}}$ and concentration decreasing as $x^{-\frac{1}{2}}$. When gravity has negligible effects, so that $B = 0$, the solution is a Gaussian plume. With finite B, there is an adverse gradient of hydrostatic pressure and the plume is decelerated so that it is deeper than in neutral flow. Numerical solutions for $\sigma = 0.71$ reveal that there is a maximum buoyancy flux B_{crit} above which no similarity solution exists. This occurs with a non-zero value of the surface velocity. For $B < B_{\text{crit}}$ it is found that there are in fact two possible solutions. One has surface velocity greater than at the critical flux and tends to the passive Gaussian plume as $B \to 0$. In the other, surface velocity decreases from B_{crit}, reaching zero at a non-zero value of B. Similar behaviour is found in an asymptotic solution for very large σ.

1. Introduction

When a heavy gas (one which is denser than air) is emitted into the atmosphere at ground level, buoyancy forces tend to make it spread sideways and upwind while at the same time the wind tries to transport it in the opposite direction. The purpose of this paper is to present some solutions of a simple, self-similar form to equations

describing this complex interaction in two dimensions. This means that we have obtained solutions to nonlinear, partial differential equations, while only having to undertake the much simpler numerical task of solving ordinary differential equations. The only simplifications needed in the incompressible, laminar Navier–Stokes equations are the Boussinesq approximation and the boundary-layer approximation. This indicates that the solutions should represent asymptotic limits of solutions of the full equations in the limit of high Reynolds number and small density differences with finite buoyancy effects.

The results are not intended to be applied quantitatively to cases of heavy-gas dispersion encountered in hazard assessment of industrial plant. For one thing, those flows are almost always turbulent. Also our solutions are confined to two-dimensional geometry while generally real plumes are free to spread transversely to the wind direction. They serve three other purposes:

(i) They make clear the interplay of physical mechanisms. This understanding can be used to guide development of integral, bulk-property models.

(ii) They can be used to test quantitively integral methods once they have been developed.

(iii) They can be used as a numerical benchmark for more complex numerical methods solving the full partial differential equations.

Although the solutions presented in this paper are for laminar flow, we have found that the solution method can be extended to certain turbulent flows as described by current higher-order closure models (Brighton 1987). Solutions for these cases will be directly applicable to certain heavy-gas flows and will also allow simple comparison of the merits of different closure schemes, and also predictions of entrainment rates from those models which can be incorporated into simple integral models.

2. Equations of motion

We imagine a constant volume flux Q of a fluid of density ρ_0 being introduced into a flowing medium of density ρ_1. The fluid is supposed to float at an upper free surface or to slump over a lower horizontal surface according to whether it is lighter or denser than the medium. We also assume that the fluid and medium are miscible with binary diffusivity D and have a common viscosity ν. Let $\Delta^* = |\rho - \rho_1|/\rho_1$ where ρ is the density field in the flow and let g^* be the acceleration due to gravity. The flow is assumed to be confined to two dimensions with horizontal coordinate x^* and velocity component u^* and vertical coordinate z^* and velocity component w^*. z^* is measured upwards or downwards according to whether the fluid is denser than the medium or not. The equations for steady, laminar, incompressible flow with the Boussinesq and boundary-layer approximations are

$$\left.\begin{aligned} u^*\frac{\partial u^*}{\partial x^*} + w^*\frac{\partial u^*}{\partial z^*} &= -\frac{1}{\rho_1}\frac{\partial p^*}{\partial x^*} + \nu\frac{\partial^2 u^*}{\partial z^{*2}}, \\ 0 &= -\frac{1}{\rho_1}\frac{\partial p^*}{\partial z^*} + g^*\Delta^*, \\ \frac{\partial u^*}{\partial x^*} + \frac{\partial w^*}{\partial z^*} &= 0, \\ u^*\frac{\partial \Delta^*}{\partial x^*} + w^*\frac{\partial \Delta^*}{\partial z^*} &= D\frac{\partial^2 \Delta^*}{\partial z^{*2}}. \end{aligned}\right\} \tag{2.1}$$

The boundary-layer approximation has been made on the assumption that horizontal lengthscales are much greater than vertical ones. The vertical momentum equation then reduces to the equation of hydrostatic balance for the pressure p^*.

3. Uniform shear upstream

3.1. *Non-dimensionalization*

Suppose there is an upstream velocity profile of the form

$$U = \Omega z^*. \tag{3.1}$$

Anticipating a solution representing an upstream intrusion, we assume a characteristic value $\Delta_0 = |\rho_0 - \rho_1|/\rho_1$ for the density field, with ρ_0 the inlet density. We take horizontal and vertical lengthscales $\mathscr{L}$ and $\mathscr{H}$ respectively. The hydrostatic equation implies $p^* \sim \rho_1 g^* \Delta_0 \mathscr{H}$ so that the terms in the momentum equation are of the magnitudes

$$\underset{\text{inertia}}{\frac{\Omega^2 \mathscr{H}^2}{\mathscr{L}}}, \quad \underset{\text{buoyancy}}{\frac{g^* \Delta_0 \mathscr{H}}{\mathscr{L}}}, \quad \underset{\text{viscosity}}{\nu \frac{\Omega}{\mathscr{H}}}.$$

Making these all the same magnitude implies

$$\mathscr{H} = g^* \Delta_0 / \Omega^2, \quad \mathscr{L} = (g^* \Delta_0)^3 / \nu \Omega^5. \tag{3.2}$$

For validity of the boundary-layer approximation, these scales must satisfy

$$\frac{\mathscr{L}}{\mathscr{H}} = \frac{(g^* \Delta_0)^2}{\nu \Omega^3} \gg 1. \tag{3.3}$$

We therefore adopt the non-dimensionalization

$$\left.\begin{aligned} x^* &= \mathscr{L} x, & z^* &= \mathscr{H} z, \\ u^* &= \Omega \mathscr{H} u, & w^* &= (\Omega \mathscr{H}^2 / \mathscr{L})\, w, \\ \Delta^* &= \Delta_0 \Delta, & p^* &= \rho_1 g^* \Delta_0 \mathscr{H} p. \end{aligned}\right\} \tag{3.4}$$

Equations (2.1) are now transformed into

$$u u_x + w u_z = -p_x + u_{zz}, \quad 0 = -p_z + \Delta, \quad u_x + w_z = 0, \quad u \Delta_x + w \Delta_z = \sigma^{-1} \Delta_{zz}, \tag{3.5}$$

where

$$\sigma = \nu / D, \tag{3.6}$$

which can be interpreted as the Prandtl or Schmidt number according to whether the density differences are caused by heat or by a contaminant.

3.2. *The form of the similarity solution*

We seek a similarity solution for u of the form

$$u = x^r f'(\eta) \quad \text{with } \eta = z/x^s, \tag{3.7}$$

where the prime denotes differentiation with respect to η so that $x^{r+s} f(\eta)$ is the stream function. To match the unperturbed flow, we need $u \sim z$ as $z \to \infty$ and so $r = s$. For inertia to balance viscosity, we find $r = \frac{1}{3}$. Hence we set

$$u = x^{\frac{1}{3}} f'(\eta), \quad \Delta = x^{\frac{1}{3}} g'(\eta), \quad p = -x^{\frac{2}{3}} g(\eta), \tag{3.8}$$

with $\eta = z/x^{\frac{1}{3}}$.

Substituting in (3.5) leads to

$$f'''+\tfrac{2}{3}ff''-\tfrac{1}{3}f'^2=\tfrac{1}{3}\eta g'-\tfrac{2}{3}g, \quad g'''+\sigma(\tfrac{2}{3}fg''-\tfrac{1}{3}f'g')=0. \tag{3.9a, b}$$

3.3. *Boundary conditions*

Three boundary conditions can immediately be imposed on the velocity profile:

$$f(0)=f'(0)=0, \quad f''(\infty)=1. \tag{3.10}$$

The first two make the surface $z=0$ a streamline with zero velocity. The third ensures that the velocity gradient achieves its unperturbed value at the top of the layer. For the buoyancy field we impose zero flux at the surface and zero concentration at infinity:

$$g''(0)=0, \quad g'(\infty)=0. \tag{3.11}$$

3.3.1. *Relation between pressure at infinity and displacement of velocity profile*

One further condition is still needed to specify the solution of the sixth-order system (3.9). To obtain this we need to appeal to the theory of perturbed laminar boundary layers. The boundary condition on f at infinity in (3.10) implies

$$f'\sim\eta-A, \quad f\sim\tfrac{1}{2}\eta^2-\eta A+B \quad \text{as } y\to\infty. \tag{3.12}$$

Substitution of these forms into (3.9a) implies

$$g(\infty)=A^2-2B. \tag{3.13}$$

A non-zero $g(\infty)$ implies that existence of a pressure gradient outside the buoyancy-driven layer and a non-zero value of A represents a displacement of the velocity profile outside the layer. In general, these two quantities are linked by the nature of the flow induced outside the boundary-layer – the displacement of the velocity profile perturbs the inviscid flow above to cause a pressure gradient which can affect the boundary-layer flow, creating a feedback loop. This phenomenon is ubiquitous in perturbed boundary layers and is described by triple-deck theory (Stewartson 1974; Smith 1982), which is associated with a natural lengthscale $R^{\frac{1}{3}}\delta$ where δ is the overall boundary-layer thickness and

$$R=U_\infty\delta/\nu\gg 1, \tag{3.14}$$

U_∞ being the free-stream speed. (In triple-deck theory, a large-scale boundary layer of thickness δ is perturbed by some disturbance which creates a much thinner inner boundary layer. This inner boundary layer corresponds to the buoyancy-driven layer in the present context.)

There are two limits in which triple-deck theory can be simplified, as discussed in detail by Smith *et al.* (1981). For disturbances on short horizontal lengthscales, $\mathscr{L}\ll R^{\frac{1}{3}}\delta$, the outer boundary-layer displacement A is forced to be zero and a non-zero pressure gradient is induced, which is determined as part of the inner-layer solution.

On large lengthscales, $\mathscr{L}\gg R^{\frac{1}{3}}\delta$, the outer boundary layer is allowed to be displaced and a pressure gradient is induced in the outer, inviscid flow but it is too small to affect the inner-layer flow.

Our similarity solutions admit either of these limiting possibilities, but the intermediate regime with the full triple-deck interaction appears not to allow a similarity form of solution. In our problem, the outer boundary-layer thickness δ and

wall-shear Ω are related by $U_\infty \sim \Omega\delta$, and so $R = \Omega\delta^2/\nu$. Hence if $\mathscr{L} \ll \Omega^{\frac{1}{4}}\delta^{\frac{3}{2}}/\nu^{\frac{1}{4}}$, we apply the sixth boundary condition

$$A = 0. \tag{3.15a}$$

If $\mathscr{L} \gg \Omega^{\frac{1}{4}}\delta^{\frac{3}{2}}/\nu^{\frac{1}{4}}$, we apply the condition

$$g(\infty) = 0. \tag{3.15b}$$

3.3.2. *The recirculatory nature of the flow*

In view of the similarity form (3.8), it appears that the point $x = 0$ represents the maximum upstream extent of a layer whose thickness and density increase downstream, presumably eventually matching on to some localized source of dense fluid. This interpretation is supported by evaluating the total buoyancy flux

$$B^* = g^* \int_0^\infty u^* \Delta^* \, \mathrm{d}z^* = g^* \Omega \mathscr{H}^2 \Delta_0 \, x \int_0^\infty f'(\eta) g'(\eta) \, \mathrm{d}\eta. \tag{3.16}$$

By integrating (3.9*b*) from 0 to ∞ and applying the boundary conditions it is readily confirmed that $B^* = 0$. The solutions represent an upstream intrusion in which buoyancy drives fluid upstream against the prevailing current, but at the same time it diffuses upwards and is carried downstream again. At the surface there must be a step change in shear from its value Ω upstream to a constant negative value $\Omega f''(0)$ for $x > 0$, as confirmed by the numerical solutions below.

3.4. *The two solutions for* $\sigma = 0.71$

3.4.1. *Numerical method*

Equations (3.9) were integrated numerically for $\sigma = 0.71$ (representing heat diffusion in air) using a subroutine from the Numerical Algorithms Group Library (NAGLIB). With boundary conditions (3.10), (3.11) and (3.15), this is a two-point boundary-value problem for which the shooting method D02HAF was used. The integration was carried out in the direction of increasing η, so one had to supply estimates of $f''(0)$, $g(0)$ and $g'(0)$ as well as the known values $f(0)$, $f'(0)$ and $g''(0)$. First a solution was obtained by imposing the conditions $f''(\eta) = 1$, $g(\eta) = 0$ at $\eta = 10$, corresponding to boundary condition (3.15*b*).

Some difficulty was experienced obtaining the solution for $A = 0$ because initial guesses at $\eta = 0$ based on the preceding solution tended to converge to the trivial solution of unperturbed shear flow. To overcome this, the strategy was adopted of taking $g'(0)$ as a fixed value instead of the condition $A = 0$. $g'(0)$ was then increased in steps from its value for the case with $g(\infty) = 0$ until A was brought down to near 0. With the boundary values on $\eta = 0$ determined in this way, the subroutine then easily converged to a non-trivial solution with $A = 0$. Since $g'(0)$ in this solution was nearly two orders of magnitude greater than for $g(\infty) = 0$, the initial difficulty was not surprising.

3.4.2. *Results*

The final results are shown in figure 1 and some key details are listed in table 1. The upstream buoyancy flux is defined by

$$B_1 = \tfrac{1}{2}x \int_0^\infty |f'(\eta)| g'(\eta) \, \mathrm{d}\eta, \tag{3.17}$$

	Boundary condition at infinity	
	Zero displacement (3.15a)	Zero pressure (3.15b)
Shear stress $f''(0)$	−1.98	−0.250
Surface pressure, $g(0)$	−4.02	−0.208
Surface concentration, $g'(0)$	3.59	0.0457
Displacement A	0	4.99
Pressure at infinity, $g(\infty)$	4.91	0
Upstream buoyancy flux, B_1/x	3.54	0.0258
Plume thickness, δ_p	2.49	4.55

TABLE 1. Main features of the similarity solutions with uniform shear flow upstream

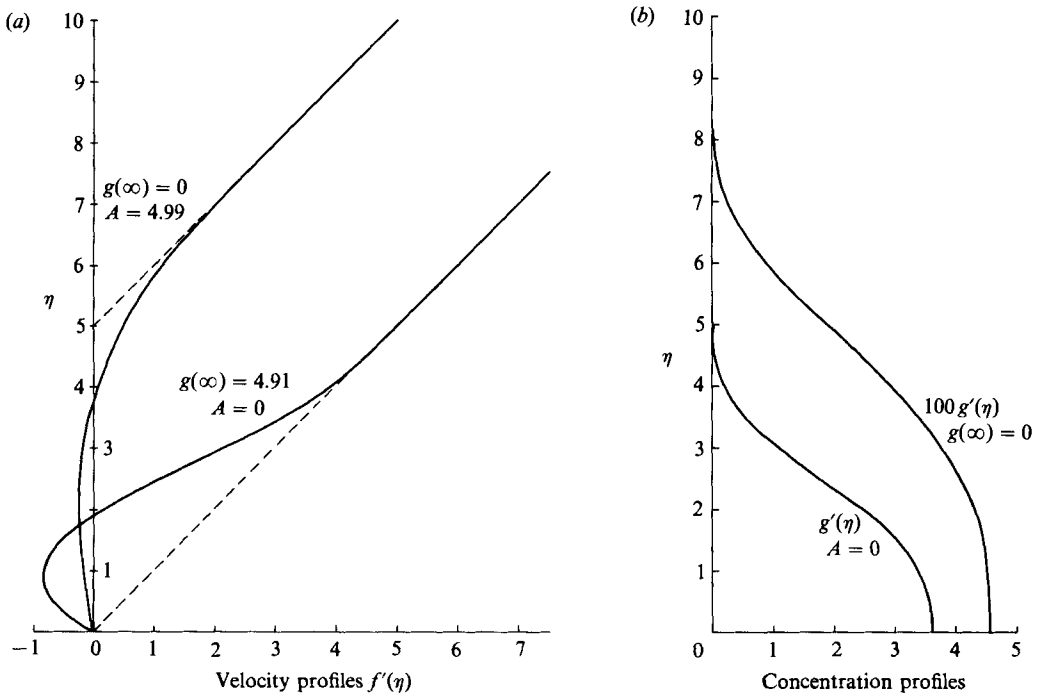

FIGURE 1. Similarity solutions with uniform shear profile upstream, for $\sigma = 0.71$. (a) Velocity profiles and (b) concentration profiles, for the alternative boundary conditions (3.15a) and (3.15b).

so it represents the amount of material flowing upstream, which is equal and opposite to that flowing downstream so that the total buoyancy flux is zero, as required by (3.16). The plume thickness is defined by

$$\delta_p = \int_0^\infty g'(\eta)\,d\eta/g'(0) = [g(\infty)-g(0)]/g'(0). \tag{3.18}$$

The remarkable difference in concentration in the two cases seems to mean that the upstream spreading of the dense material is very sensitive to the exterior flow conditions. When the external flow is readily displaced out of the way, only a small density difference is required to maintain a region of nearly stagnant dense fluid. If

the external flow cannot be displaced, a much larger density difference is needed to drive fluid upstream and the wall flow has more of a jet-like character with an inflection point where the velocity gradient exceeds that in the outer flow (see figure 1). The properties of the solutions in dimensional and quantitative terms are discussed below.

3.5. *Solution for large Schmidt or Prandtl number*

In water-channel studies of heavy-gas dispersion, salt is often used to produce the density difference. This has a Schmidt number of 1035 at 15 °C whereas Schmidt numbers for gases in air are generally in the range 0.6–3, so it is useful to determine the behaviour of the similarity solutions over a large range of σ. For $\sigma \gg 1$, the equations and boundary conditions can be rescaled straightforwardly by the transformation

$$\eta = \sigma^{-\frac{1}{3}}\tilde{\eta}, \quad f = \sigma^{-\frac{2}{3}}\tilde{f}(\tilde{\eta}), \quad g(\eta) = \sigma^{\frac{1}{3}}\tilde{g}(\tilde{\eta}), \tag{3.19}$$

so that (3.9) become

$$\tilde{f}''' + \sigma^{-1}(\tfrac{2}{3}\tilde{f}\tilde{f}'' - \tfrac{1}{3}\tilde{f}'^2) = \tfrac{1}{3}\tilde{\eta}\tilde{g}' - \tfrac{2}{3}\tilde{g}, \quad \tilde{g}''' + \tfrac{2}{3}\tilde{f}\tilde{g}'' - \tfrac{1}{3}\tilde{f}'\tilde{g}' = 0, \tag{3.20a, b}$$

while boundary conditions (3.10), (3.11) and (3.15) remain unchanged. The physical interpretation of this scaling is that the layer thickness is determined by diffusivity, a balance of diffusion with advection, rather than of viscous stresses with inertia.

Rescaled in this form, the equations have been solved numerically for a range of values of σ including the limiting case $\sigma^{-1} = 0$. Profiles for the values $\sigma = 1$ and $\sigma^{-1} = 0$ are compared in figure 2 for the zero-pressure boundary condition. From (3.20a), it is seen that in the rescaled problem, σ^{-1} appears only as the coefficient of the inertia terms in the momentum equation. From figure 2(a) it is seen that the resultant velocity profiles are fairly similar but in the 'inertialess' case, a considerably larger density difference is needed to drive the flow (see figure 2b). Figure 3 shows the variation with σ of the main features of the solution as listed in table 1.

3.6. *Overall properties of the flow in dimensional terms*

This similarity solution appears to represent a wedge of dense fluid extending upstream from some kind of source. The overall flow is illustrated in physical terms in figure 4, where (3.4) has been used to restore variables to dimensional form. Relative to the leading edge of the dense layer as origin for x^*, the plume thickness varies as

$$\delta_{\mathrm{p}}^* = (\nu x^*/\Omega)^{\frac{1}{3}}\delta_{\mathrm{p}}, \tag{3.21}$$

where δ_{p} is the number defined by (3.18). The maximum reversed velocity in the layer is given by

$$(-u^*)_{\max} = (\Omega^2\nu x^*)^{\frac{1}{3}} \max\,[-f'(\eta)]. \tag{3.22}$$

The concentration at the surface varies as

$$\Delta^*|_{z=0} = (\Omega^5\nu x^*/g^{*3})^{\frac{1}{3}}g'(0), \tag{3.23}$$

and the upstream buoyancy flux is

$$B_1^* = \Omega^2\nu x^*(B_1/x), \tag{3.24}$$

with B_1/x given by (3.17) with values shown in table 1 and figure 3.

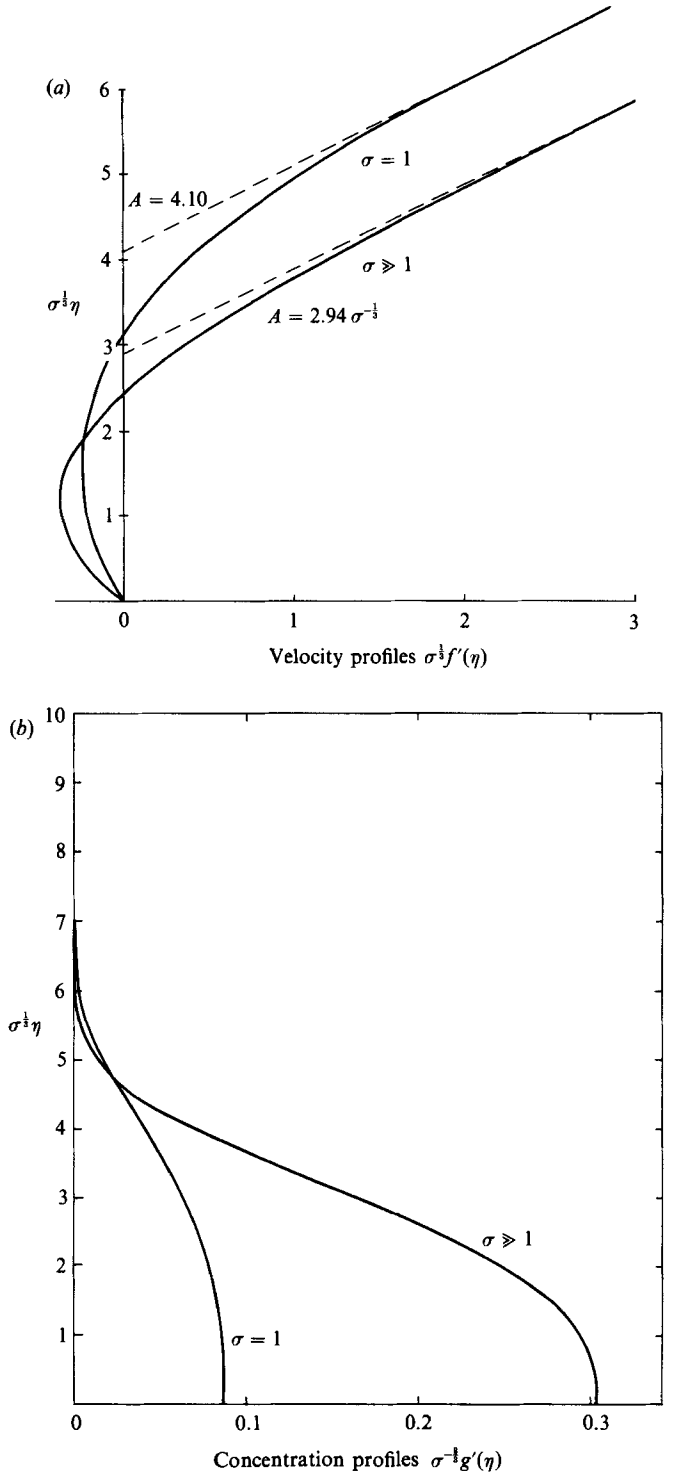

FIGURE 2. Similarity solutions with uniform shear profile upstream, for $\sigma = 1$ and $\sigma \to \infty$, for boundary conditions $g(\infty) = 0$. (*a*) Velocity profiles, (*b*) concentration profiles.

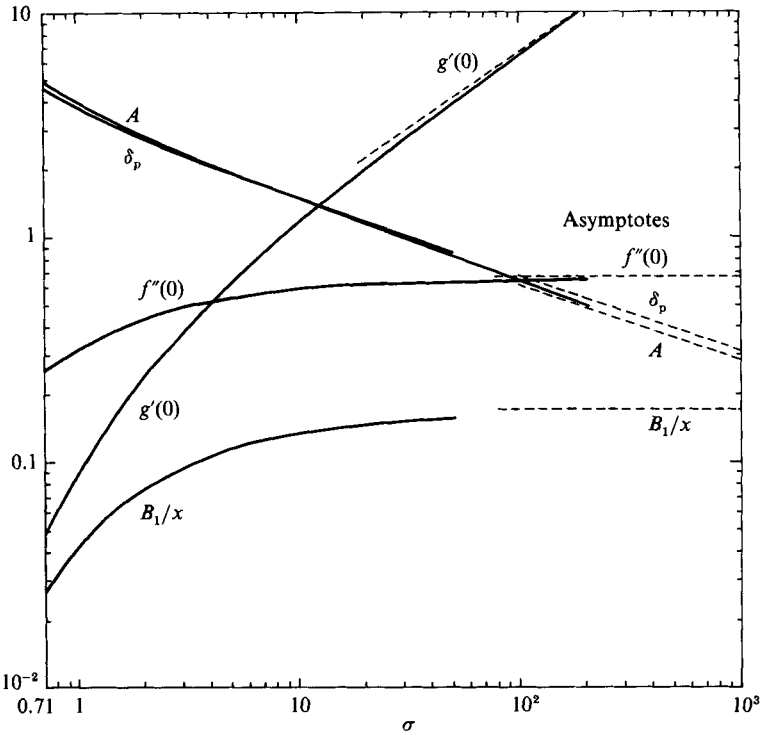

FIGURE 3. Variation with σ of properties of the similarity solution with uniform shear profile upstream for $g(\infty) = 0$.

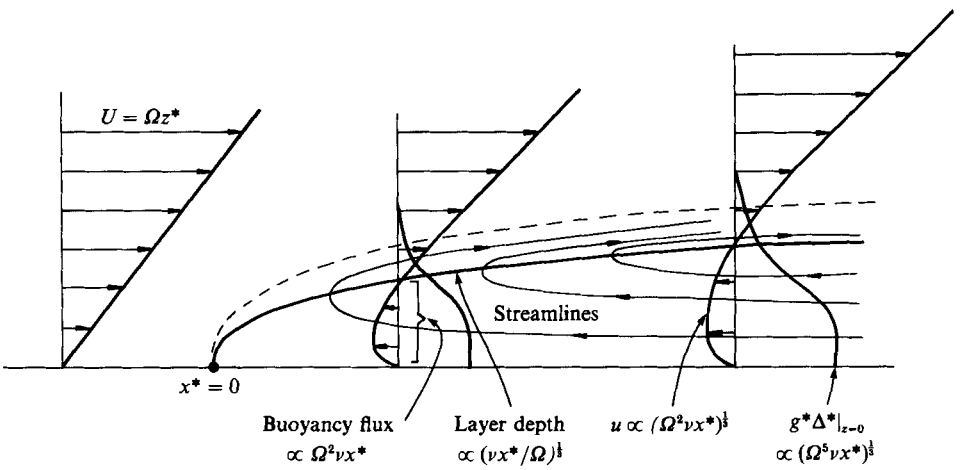

FIGURE 4. Qualitative sketch of the flow field represented by the similarity solution for uniform shear flow upstream.

3.6.1. *Fitting the similarity solution to the rest of the flow field*

This similarity solution cannot represent a complete flow because the density increases without limit downstream. Can this form of stationary recirculatory wedge of fluid be set up with a suitable form of inflow downstream ? This question cannot be answered without a detailed analysis of the whole flow domain, but it seems a reasonable hypothesis that this flow could form upstream of an isolated continuous

steady source of dense fluid located in the horizontal surface. If this has density difference Δ_0 we may enquire what size of upstream wedge is needed to achieve this density at the location of the source (this is only a rough estimate as the flow near the source must have a non-self-similar character). Setting $\Delta^*|_{z=0} = \Delta_0$ in (3.23) and solving for x^* gives an estimate of the upstream extent of the current

$$x_c^* = \frac{1}{\Omega^5 \nu}\left(\frac{g^* \Delta_0}{g'(0)}\right)^3. \tag{3.25}$$

This result is rather remarkable because of the very strong dependence on the unperturbed shear stress Ω. There is also an extreme sensitivity to the choice of the pressure boundary condition (3.15). For zero pressure x_c^* is a factor 4.8×10^5 greater than for zero displacement for $\sigma = 0.71$, from the results in table 1.

There is no direct dependence on the buoyancy flux at the source in these two solutions, which seems rather counter to intuition. However, we can evaluate the upstream buoyancy flux as given by (3.24) at $x^* = x_c^*$ to obtain

$$B_{1c}^* = \frac{1}{\Omega^3}\left(\frac{g^* \Delta_0}{g'(0)}\right)^3 \left(\frac{B_1}{x}\right). \tag{3.26}$$

For the zero-pressure boundary condition B_{1c}^* is a factor 3.50×10^3 greater than for the zero-displacement condition with $\sigma = 0.71$. This upstream buoyancy flux cannot be directly linked to the source buoyancy flux, because some of the dense fluid at the source may proceed directly downstream, and some of the downstream flux in the intrusion may be recirculated into the upstream flow, for instance if there is a barrier just downstream of the source. For emission from a source flush with the surface the second possibility seems unlikely, and B_{1c}^* would be directly related to the source strength. Intrusions of intermediate length involving the full triple-deck interaction (and therefore non-self-similar) could be formed for intermediate values of B_{1c}^*. A full numerical treatment or an experimental investigation would be needed to explore this further.

3.6.2. *Examples for laboratory conditions*

To illustrate the possible relevance of these solutions in laboratory conditions, we have evaluated x_c^* from (3.25) for a few cases.

For a laminar boundary layer in an airstream of velocity $U_\infty = 1\ \mathrm{m\ s^{-1}}$, with viscosity $\nu = 1.5 \times 10^{-5}\ \mathrm{m^2\ s^{-1}}$, a Reynolds number R of 10^3 corresponds to $\delta = 1.5 \times 10^{-2}$ m. Taking $\Omega = U_\infty/\delta$ and $g^* \Delta_0 = 1\ \mathrm{m\ s^{-2}}$ gives $x_c^* = 5.1 \times 10^{-5}/[g'(0)]^3$ in metres. From table 1 this gives $x_c^* = 0.53$ m for the zero-pressure condition and $x_c^* = 1.1 \times 10^{-6}$ m for the zero-displacement condition. Both results are consistent with the triple-deck lengthscale $R^{\frac{1}{4}}\delta$, which is 0.084 m. The dimensional plume thickness in terms of x_c^* is

$$\delta_p^* = \frac{g^* \Delta_0}{\Omega^2} \frac{\delta_p}{g'(0)}, \tag{3.27}$$

from (3.21) and (3.25). For the first case this is 2.2×10^{-2} m which is consistent with the boundary-layer approximation in the buoyancy-driven layer. For the second case, with zero displacement, $\delta_p^* = 1.0 \times 10^{-2}$ m, so the solution is not self-consistent, but does imply that the upstream spreading will be negligible in extent. The upstream buoyancy flux B_{1c}^* for the zero-pressure condition corresponds to a flow rate $B_{1c}^*/g^* \Delta_0$ of $9.2 \times 10^{-4}\ \mathrm{m^2/s}$.

For a brine inflow in water ($\sigma \approx 1000$), $-g'(0)$ takes the asymptotic value $0.303\sigma^{\frac{2}{3}} = 31$ from figure 3. With $\nu = 10^{-6}$ m^2 s^{-1} and $U_\infty = 0.1$ m s^{-1}, a Reynolds number R of 1000 implies $\delta = 10^{-2}$ m and so we take $\Omega = 10$ s^{-1}. With $g^*\Delta_0 = 1$ m s^{-2}, $x_c^* = 3.4 \times 10^{-4}$ m even for the zero-pressure case and so the upstream spreading is negligible.

The great sensitivity to Ω in (3.25) means that only a modest change in conditions is needed to give a significant result. With $U_\infty = 0.06$ m s^{-1} and $\delta = 0.03$ m to give $R = 1800$, we have $\Omega = U_\infty/\delta = 2$ s^{-1}. With the same value of $g^*\Delta_0$, we obtain $x_c^* = 1.0$ m for the zero-pressure case with $\delta_p^* = 2.5 \times 10^{-3}$ m. Since the triple-deck lengthscale here is 0.20 m all the conditions of the analysis are fairly well achieved. The upstream flow rate of dense fluid $B_{1c}^*/g^*\Delta_0$ is 7.1×10^{-7} m^2/s.

Thus conditions needed for the occurrence of the similarity solutions should be readily achievable in the laboratory.

3.6.3. *Experiments on arrested saline wedges*

The only experiments approaching the conditions described above are those on stationary gravity currents of salty water as a model of a river flow interacting with intruding sea water. A detailed laboratory model study of these is described by Riddell (1970). In one set of experiments, he introduced an upstream flow of salt water into a turbulent channel flow at a Reynolds number of 5440, low enough for there to be a thick laminar sublayer in which one might observe a laminar wedge at the upstream tip. Riddell measured interface heights as a function of horizontal position, by unspecified means, presumably by eye. The results have some qualitative features of our similarity solutions. For varying salt in flow rates, the length of the wedge varied but the tip portion always had the same profile, well approximated by a parabolic or cubic curve. The channel depth was 0.1016 m and the wedge reached a thickness of 1.5×10^{-2} m in a distance of about 0.96 m from the tip. This is about ten times the value of δ_p^* obtained from (3.21) where Ω is taken as the value of the shear in the laminar sublayer u_*^2/ν, with u_* the friction velocity. u_* was 3.2×10^{-3} m s^{-1} giving $\Omega = 9.9$ s^{-1} and the laminar sublayer thickness was therefore $5\nu/u_* = 1.6 \times 10^{-3}$ m, much smaller than the current depth. So turbulence may have had a major role in forming even the thin leading edges of Riddell's saline wedges.

4. Uniform velocity upstream with a free surface

4.1. *Non-dimensionalization*

The other similarity solution that we have found has a uniform flow velocity U outside the gravity current. This would be realized physically by flow at a horizontal free surface and so the gravity current solutions could represent warm water discharged at the surface of cold, or fresh water flowing into salty.

The dimensional arguments of §3.1 were based on seeking a horizontal lengthscale $\mathscr{L}$ for upstream spreading to be associated with a given imposed density difference Δ_0. To apply this analysis in this case $\Omega\mathscr{H}$ is replaced by U and instead of (3.2) one finds

$$\mathscr{H} = U^2/g^*\Delta_0, \quad \mathscr{L} = U^5/\nu(g^*\Delta_0)^2. \tag{4.1}$$

This leads to the absurd conclusion that the gravity current increases in length if the density is decreased or the flow velocity increased.

The scaling does make sense however if it is applied to flow downstream from a

source. Then Δ_0 can be interpreted as the density difference at some given distance $\mathscr{L}$ and we have instead of (4.1)

$$\mathscr{H} = (\nu\mathscr{L}/U)^{\frac{1}{2}}, \quad g^*\Delta_0 \sim U^{\frac{5}{2}}/(\nu\mathscr{L})^{\frac{1}{2}}. \tag{4.2}$$

The layer thickness is the familiar scaling of the flat-plate boundary layer. We therefore adopt the following non-dimensionalization:

$$\left.\begin{aligned} x^* = \mathscr{L}x, \quad z^* = \mathscr{H}z, \\ u^* = Uu, \quad w^* = (U\mathscr{H}/\mathscr{L})w, \\ \Delta^* = [U^{\frac{5}{2}}/g^*(\nu\mathscr{L})^{\frac{1}{2}}]\Delta, \quad p^* = \rho_1 U^2 p. \end{aligned}\right\} \tag{4.3}$$

The non-dimensional form (3.5) of the equations of motion still applies.

Note that Δ_0 is an arbitrary choice, purely a measuring scale. If Δ_0 is replaced by $\alpha\Delta_0$, $\mathscr{L}$ by $\alpha^{-2}\mathscr{L}$ and $\mathscr{H}$ by $\alpha^{-1}\mathscr{H}$ then the dimensionless equations remain the same.

4.2. *The form of the similarity solution*

Using (3.7) for the velocity distribution, we can first set $r = 0$ to ensure matching with the uniform flow when $\eta \to \infty$. The inertia–viscous balance now requires $s = \frac{1}{2}$ as for the flat-plate boundary layer. The definitions of the similarity profiles become

$$u = f'(\eta), \quad \Delta = x^{-\frac{1}{2}}/g'(\eta), \quad p = -g(\eta), \tag{4.4}$$

with

$$\eta = z/x^{\frac{1}{2}}.$$

The concentration Δ now decays with distance instead of increasing as for the shear profile in (3.8). This confirms that the solutions will represent a dense downstream plume. The momentum and advection–diffusion equations become

$$f''' + \tfrac{1}{2}ff'' = \tfrac{1}{2}\eta g', \quad g''' + \tfrac{1}{2}\sigma(fg'' + f'g') = 0. \tag{4.5a, b}$$

4.3. *Boundary conditions*

The boundary conditions on the velocity profile are:

$$f(0) = f''(0) = 0, \quad f'(\infty) = 1. \tag{4.6}$$

The first ensures zero vertical velocity at the surface, the second zero shear stress there and the third ensures matching with the free-stream velocity. For the concentration profile there are two conditions:

$$g''(0) = 0, \quad g(\infty) = 0, \tag{4.7}$$

giving zero surface flux and zero pressure and concentration at infinity. These conditions can be used to integrate (4.5b) once to give

$$g'' + \tfrac{1}{2}\sigma fg' = 0. \tag{4.8}$$

Indeed this can be solved to give g' explicitly as

$$g' = g'(0)\exp\left(-\tfrac{1}{2}\sigma\int_0^\eta f(\eta)\,\mathrm{d}\eta\right), \tag{4.9}$$

but the form (4.8) is more convenient for numerical solution.

4.3.1. *The buoyancy flux*

To obtain a sixth condition for (4.5), we need to specify the total buoyancy flux in the plume:

$$B = \int_0^\infty f'g' \, d\eta. \tag{4.10}$$

This quantity is regarded as a free parameter so that there is a range of similarity solutions for varying B. In dimensional terms

$$B = g^* \int_0^\infty u^* \Delta^* \, dz^*/U^3, \tag{4.11}$$

i.e. the dimensionless buoyancy flux per unit width.

That B is a constant independent of x is seen by integrating (4.5*b*) from 0 to ∞ and applying the boundary conditions.

4.4. *Solutions with small buoyancy flux*

The parameter B expresses the ratio of buoyancy and inertia forces in the plume. When $B \ll 1$, one expects the plume to behave passively, i.e. to undergo advection and diffusion without affecting the velocity field significantly. To verify this explicitly it is convenient to set $g'(0) = \beta$ and take the limit $\beta \to 0$. The velocity and concentration profiles are expanded as

$$f(\eta) = \eta + \beta f_1(\eta) + O(\beta^2), \quad g(\eta) = \beta g_1(\eta) + O(\beta^2). \tag{4.12}$$

From (4.9), we find that the concentration has the passive Gaussian profile

$$g_1'(\eta) = e^{-\frac{1}{4}\sigma\eta^2}. \tag{4.13}$$

Hence the buoyancy flux (4.10) is given by

$$B = \beta \int_0^\infty g_1'(\eta) \, d\eta + O(\beta^2) = \beta\pi^{\frac{1}{2}}/\sigma. \tag{4.14}$$

The solution for f_1 is useful for illustrating the influence of σ on the velocity field. It satisfies the linearized form of (4.5*a*):

$$f_1''' + \tfrac{1}{2}\eta f_1'' = \tfrac{1}{2}\eta \, e^{-\frac{1}{4}\sigma\eta^2}, \tag{4.15}$$

and boundary conditions

$$f_1(0) = f_1''(0) = 0, \quad f_1'(\infty) = 0. \tag{4.16}$$

The complete velocity profile is given by

$$\left.\begin{aligned} f' &= 1 - \frac{\beta\pi^{\frac{1}{2}}}{1-\sigma}\left[\frac{1}{\sigma^{\frac{1}{2}}}\operatorname{erfc}(\tfrac{1}{2}\sigma^{\frac{1}{2}}\eta) - \operatorname{erfc}(\tfrac{1}{2}\eta)\right] + O(\beta^2) \quad \text{for } \sigma \neq 1, \\ &= 1 - \tfrac{1}{2}\beta[\eta \, e^{-\frac{1}{4}\eta^2} + \pi^{\frac{1}{2}} \operatorname{erfc}(\tfrac{1}{2}\eta)] + O(\beta^2) \quad \text{for } \sigma = 1. \end{aligned}\right\} \tag{4.17}$$

The surface velocity is given by

$$f'(0) = 1 - \frac{\pi^{\frac{1}{2}}\beta}{\sigma^{\frac{1}{2}}(1+\sigma^{\frac{1}{2}})} + O(\beta^2). \tag{4.18}$$

From (4.17), it is seen that the buoyancy of the plume causes it to slow down at the surface – the horizontal gradient of hydrostatic pressure is adverse. At large σ the

plume itself is confined to a depth of $O(\sigma^{-\frac{1}{2}})$ but the fluid outside the plume is slowed down by viscous effects over a vertical scale of $O(1)$. At small σ the diffusion of matter is much faster than that of momentum and the hydrostatic pressure drives an inviscid flow on the scale $\eta = O(\sigma^{-\frac{1}{2}})$ with a thin viscous adjustment region of $O(1)$ thickness to accommodate the zero shear stress condition at $\eta = 0$.

4.5. *Numerical solutions for* $\sigma = 0.71$

Equations (4.5*a*) and (4.8) were solved numerically using the NAGLIB shooting-method algorithm D02HAF, already used for the shear-flow problem. The constraint (4.10) fixing the buoyancy flux at a desired value was not convenient for the numerical method; instead the inverse procedure was adopted of fixing the surface concentration $g'(0)$ and determining B from the solution. Thus $f(0)$, $f''(0)$ and $g'(0)$ were regarded as known initial values for the fourth-order problem (note that g does not have to be solved for) and the shooting technique was directed at satisfying $f'(\infty) = 1$. (The condition $g'(\infty) = 0$ is satisfied automatically in view of (4.9).) The calculation was started at small values of $g'(0)$ for which $f'(0)$ could be estimated from the linearized solution of §4.4 in order to start the algorithm off.

This method was only successful up to a point: it proved impossible to find solutions beyond $g'(0) = 0.192$ when $f'(0) = 0.564$. The nature of the difficulty was revealed by using $f'(0)$ as the specified variable and letting $g'(0)$ vary in order to satisfy the condition at infinity. Solutions were found for $f'(0)$ decreasing to zero, for which $g'(0)$ and B also decreased. In other words there exists a maximum possible buoyancy flux $B = 0.341$ above which there is no solution to the similarity equations and below which there are two.

4.5.1. *Velocity and concentration profiles*

Figure 5 shows velocity and concentration profiles in what we have termed the 'supercritical' mode with the surface velocity reduction intermediate between 0 as for a passive plume and the value of 0.564 at the maximum buoyancy flux.

In figure 6 we show that there are also solutions down to $f'(0) = 0$ in which decreases of buoyancy flux are associated with increases in the surface velocity reduction. In this 'subcritical' mode there is a distinct deepening of the plume and flattening of the concentration profile. Solutions can also be computed for $f'(0) < 0$ but these are physically meaningless near the surface $\eta = 0$.

Figure 7 summarizes the variation of key flow properties with buoyancy flux. The plume depth can be characterized in several ways: the displacement thickness, defined as in classical boundary-layer theory, is

$$\delta_1 = \int_0^\infty (1-f')\,\mathrm{d}\eta = \lim_{\eta\to\infty}[\eta - f(\eta)]. \tag{4.19}$$

The width of the velocity profile can be defined by

$$\delta_2 = \delta_1/[1-f'(0)]. \tag{4.20}$$

The plume depth is given as in (3.18) by

$$\delta_\mathrm{p} = \int_0^\infty g'(\eta)\,\mathrm{d}\eta/g'(0). \tag{4.21}$$

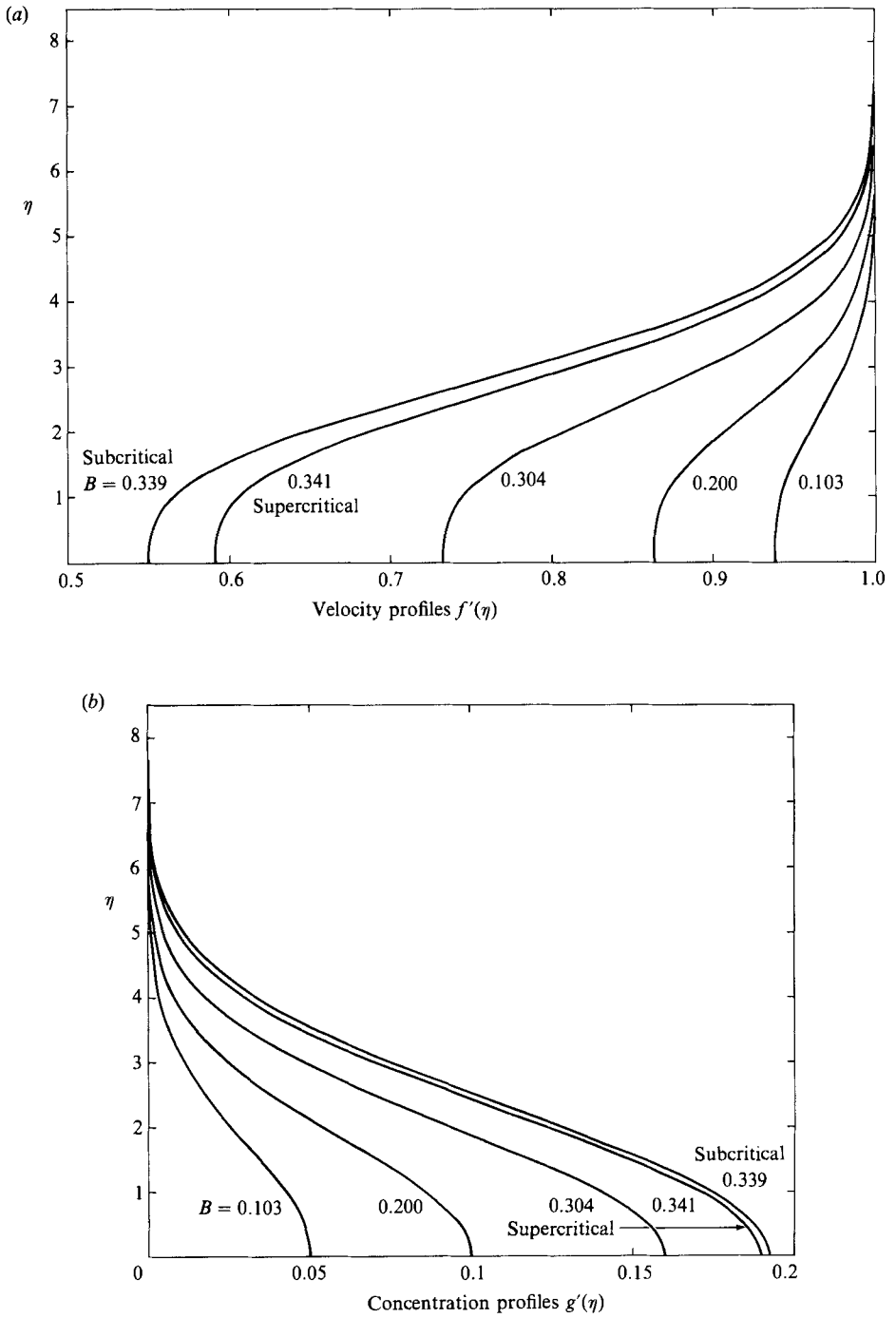

FIGURE 5. Similarity solutions with uniform flow upstream, for $\sigma = 0.71$. (*a*) Velocity profiles and (*b*) concentration profiles, for the supercritical mode.

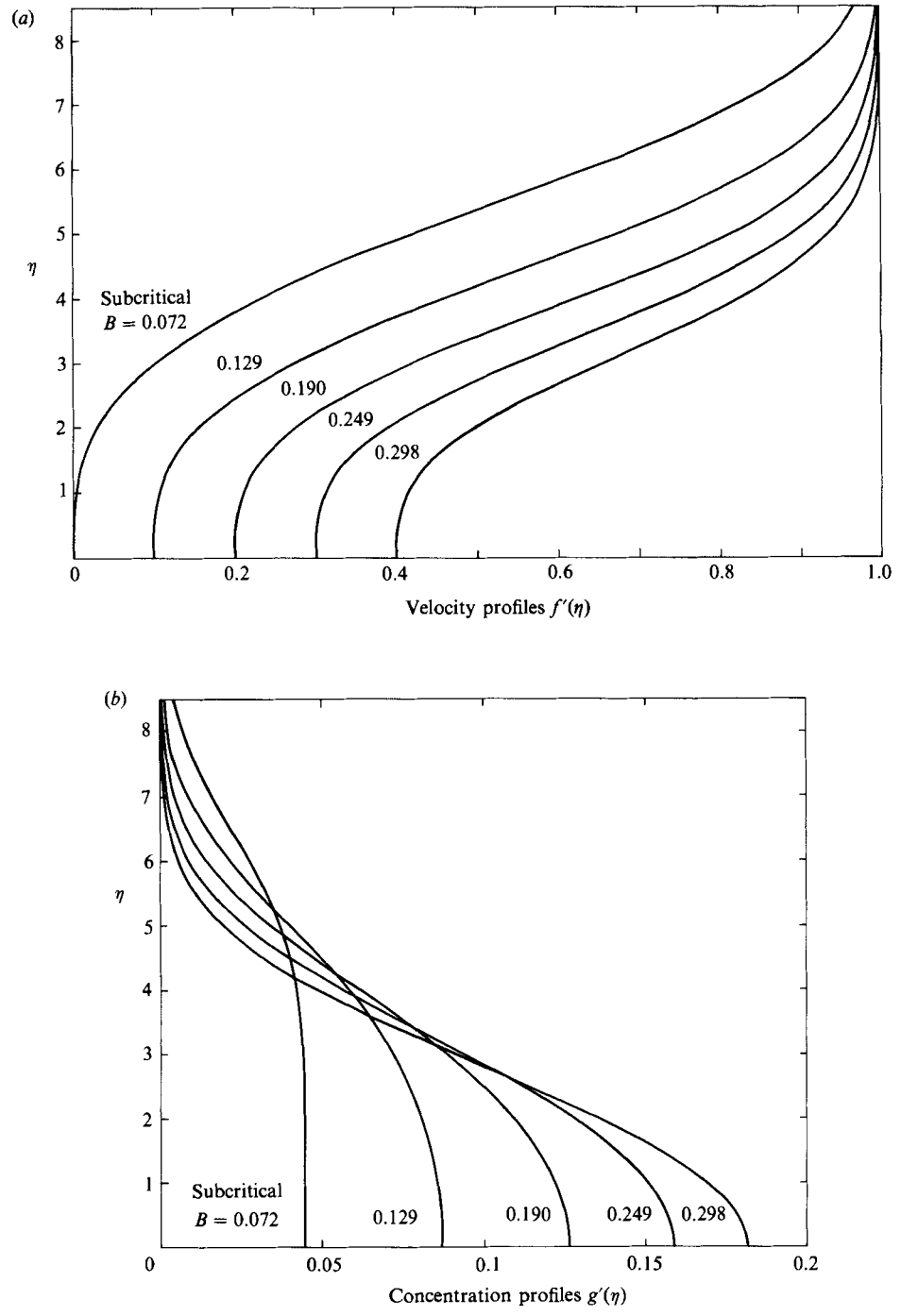

FIGURE 6. Similarity solutions with uniform flow upstream, for $\sigma = 0.71$. (*a*) Velocity profiles and (*b*) concentration profiles, for the subcritical mode.

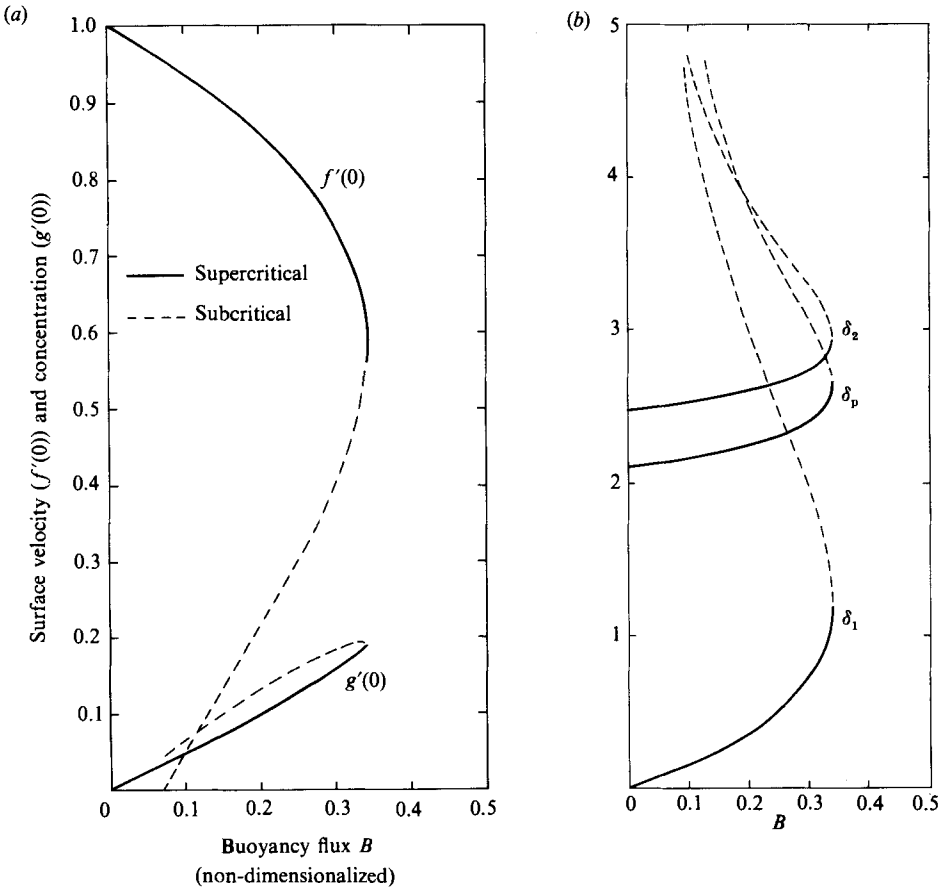

FIGURE 7. Uniform flow upstream. Variation of (*a*) surface velocity and surface concentration and (*b*) displacement thickness, velocity profile width and plume thickness, with the buoyancy parameter B for $\sigma = 0.71$.

4.6. *Solution for large Schmidt or Prandtl number*

The solution for nearly passive flow in §4.4 revealed the essential structure for the case $\sigma \gg 1$. The slowly diffusing contaminant remains confined to a thin layer of thickness $O(\sigma^{-\frac{1}{2}})$ in which the flow is dominated by viscosity. In the outer layer, for $\eta = O(1)$, gravitational effects are absent except for $\eta \to 0$. This can be described by matched asymptotic expansions.

In the inner layer, the problem is rescaled by defining

$$\bar{\eta} = \sigma^{\frac{1}{2}}\eta, \tag{4.22}$$

and the solutions are expanded in powers of $\sigma^{-\frac{1}{2}}$:

$$f(\eta) = \sigma^{-\frac{1}{2}}\bar{f}_1(\bar{\eta}) + \sigma^{-1}\bar{f}_2(\bar{\eta}) + O(\sigma^{-\frac{3}{2}}), \quad g(\eta) = \sigma^{\frac{1}{2}}\bar{g}_1(\bar{\eta}) + O(1). \tag{4.23}$$

Equations (4.5*a*) and (4.8) yield

$$\bar{f}_1''' = 0, \quad \bar{f}_2''' = \tfrac{1}{2}\bar{\eta}\bar{g}_1', \quad \bar{g}_1'' + \tfrac{1}{2}\bar{f}_1\bar{g}_1 = 0. \tag{4.24a–c}$$

The solutions satisfying $\bar{f}_i(0) = \bar{f}_i''(0) = 0$ for $i = 1, 2$ and $\bar{g}_1'(\infty) = 0$ are

$$\bar{f}_1 = \alpha_1 \bar{\eta}, \quad \bar{f}_2'' = \frac{\gamma}{\alpha_1}(1 - \mathrm{e}^{-\frac{1}{4}\alpha_1 \bar{\eta}^2}), \quad \bar{g}_1' = \gamma\, \mathrm{e}^{-\frac{1}{4}\alpha_1 \bar{\eta}^2}. \tag{4.25a–c}$$

To lowest order the flow is a uniform velocity α_1 and the concentration has a Gaussian profile with (scaled) surface concentration γ.

To relate α_1 and γ to the imposed buoyancy flux, we have to solve the problem in the outer region where g is exponentially small and so f satisfies the classical Blasius equation

$$f''' + \tfrac{1}{2} f f'' = 0. \tag{4.26}$$

To match to the inner region, consider the small-η behaviour:

$$f \sim \alpha_1 \eta + \tfrac{1}{2}\alpha_2 \eta^2 + O(\eta^3) \quad \text{as } \eta \to 0. \tag{4.27}$$

In the inner variables this can be written as

$$f \sim \sigma^{-\frac{1}{2}}\alpha_1 \bar{\eta} + \tfrac{1}{2}\sigma^{-1}\alpha_2 \bar{\eta}^2 + O(\sigma^{-\frac{3}{2}}). \tag{4.28}$$

The first term matches the solution (4.25a) while the second term matches (4.25b) if

$$\gamma = \alpha_1 \alpha_2. \tag{4.29}$$

This now gives an algorithm for generating these large-σ solutions numerically. The Blasius problem (4.26) is solved for given values of $f'(0) = \alpha_1$ and $\alpha_2 = f''(0)$ is determined as part of the solution. Equation (4.29) then gives the surface concentration and the overall plume properties are obtained as

$$g'(0) = \sigma\alpha_1\alpha_2 + O(\sigma^{\frac{1}{2}}), \tag{4.30a}$$

$$\begin{aligned} B &= \sigma^{\frac{1}{2}} \int_0^\infty \bar{f}_1'(\bar{\eta})\, \bar{g}_1'(\bar{\eta})\, \mathrm{d}\bar{\eta} + O(1) \\ &= \sigma^{\frac{1}{2}} \pi^{\frac{1}{2}} \alpha_1^{\frac{3}{2}} \alpha_2 + O(1), \end{aligned} \tag{4.30b}$$

$$\delta_1 = \int_1^\infty [1 - f'(\eta)]\, \mathrm{d}\eta + O(\sigma^{-\frac{1}{2}}), \tag{4.30c}$$

$$\delta_2 = \delta_1/(1 - \alpha_1) + O(\sigma^{-\frac{1}{2}}), \tag{4.30d}$$

$$\delta_\mathrm{p} = \sigma^{-\frac{1}{2}} \pi^{\frac{1}{2}} \alpha_1^{\frac{1}{2}} + O(\sigma^{-1}). \tag{4.30e}$$

These results are consistent with those of §4.4 when $\gamma \ll 1$.

Figure 8 shows the variation of the basic flow parameters (4.30) with B for supercritical and subcritical plumes. The form of the curves for $f'(0)$ and $g'(0)$ is very similar for $\sigma = 0.71$ in figure 7, except that the critical buoyancy flux is given by $B = 0.16\sigma^{\frac{1}{2}}$. The layer thickness in figure 8(b) has a somewhat different form because as $B \to 0$ for the subcritical flow, so also $\alpha_1 \to 0$ in (4.26) and the solution becomes the flat-plate Blasius solution itself with finite displacement thickness $\delta_1 = 1.821$ and shear $\alpha_2 = 0.3321$. In fact this is a singular limit with $\delta_\mathrm{p} \to \infty$ because the zero velocity at the surface invalidates the scaling arguments for the inner boundary layer. However this very special case is not explored further here.

4.7. *Solutions with zero velocity at the surface*

In the problem defined by (4.5a) and (4.8) with boundary conditions (4.6) and (4.7), it is possible to replace the boundary conditions on $f''(0)$ by the no-slip condition

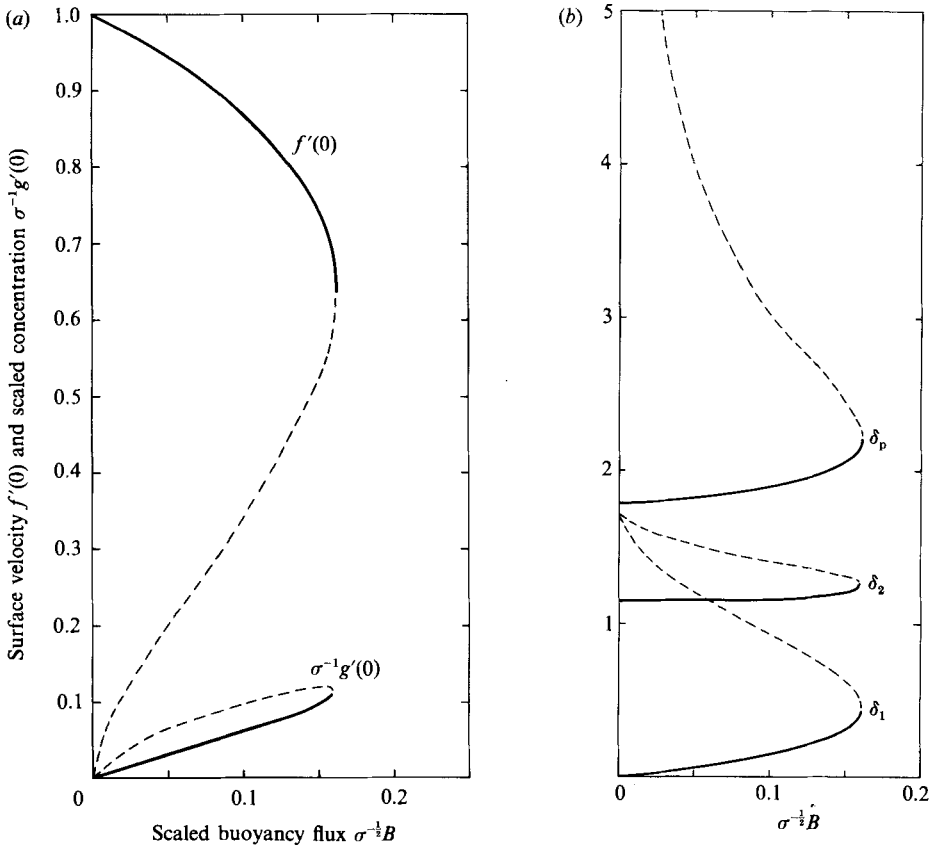

FIGURE 8. Uniform flow upstream. Variation of (*a*) surface velocity and surface concentration and (*b*) displacement thickness, velocity profile width and plume thickness with the buoyancy parameter B for the asymptotic solution in the limit $\sigma \to \infty$.

σ	Critical buoyancy flux B	Critical surface concentration $g'(0)$
0.5	0.113	0.058
0.1	0.102	0.079
2.0	0.090	0.110
6.8	0.084	0.217

TABLE 2. Results for the no-slip case from Schneider (1979) and Afzal & Hussain (1984)

$f'(0) = 0$. This represents emission of the buoyant material at the leading edge of a flat plate and in this case increasing B causes perturbations from the Blasius solution. This problem has been solved numerically by Gill & del Casal (1962) and Schneider (1979), as a combined forced and free heat convection problem in which the temperature of a horizontal flat plate is inversely proportional to the square root of the distance from the leading edge.

Schneider (1979) discovered that there was a maximum value of the negative buoyancy beyond which solutions did not exist. Later Afzal & Hussain (1984) and de Hoog, Laminger & Weiss (1984) discovered the existence of the second, subcritical solution. The results of these authors are summarized in table 2 after conversion to

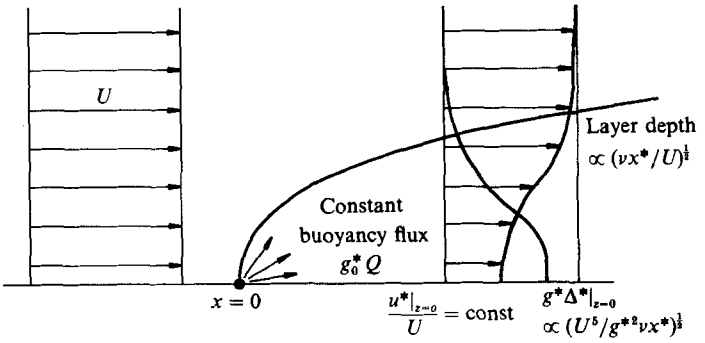

FIGURE 9. Qualitative sketch of the flow field represented by the similarity solution for uniform flow upstream.

our notation. It is seen from table 2 that the critical buoyancy fluxes are smaller in this case, perhaps because the plume is being emitted into a slower-moving flow. The trend with increasing σ appears to be opposite to that for our free-surface case, as in (4.30*b*), but it appears that the large-σ analysis has not been carried out for the no-slip case.

4.8. *Overall properties of the flow in dimensional terms*

Unlike the similarity solution for the shear profile upstream, this solution appears to represent a complete flow field downstream of a source of buoyancy near a horizontal free surface. Figure 9 is a schematic diagram of the overall flow field from which it is seen that the parameter B is related to the source volume flux per unit width by

$$B = g^*(\rho_0/\rho_1 - 1)\, Q/U^3. \tag{4.31}$$

The dimensional plume thickness is given by

$$\delta_p^* = \delta_p(\nu x^*/U)^{\frac{1}{2}}, \tag{4.32}$$

and it is perhaps noteworthy that as buoyancy increases so also the plume thickness increases (see figures 7 and 8). The density difference at the surface is given by

$$\Delta^* = (U^{\frac{5}{2}}/g^*\nu^{\frac{1}{2}}x^{*\frac{1}{2}})\, g'(0). \tag{4.33}$$

The gradient Richardson number is also of interest for questions of flow stability. It is given by

$$Ri = \frac{g^*\partial\Delta^*/\partial z^*}{(\partial u^*/\partial z^*)^2} = \frac{g''(\eta)}{[f''(\eta)]^2}. \tag{4.34}$$

Thus the maximum Richardson number remains a constant downstream. Buoyancy effects remain of equal significance no matter how much dilution occurs.

4.8.1. *Flow near the source*

The parabolic plume profile means that in fact the boundary-layer assumptions break down near the source where $x^* = 0$. Since the density (4.33) becomes infinite there, it is clear that a local solution of the full Navier–Stokes equations would be needed to resolve the flow structure there. This is just the same difficulty as arises in the solution for the flat-plate boundary layer at the leading edge and there is no reason to expect that it would affect the validity of the similarity solution downstream where x^* is much greater than the source dimensions and the Reynolds number Ux^*/ν is large.

4.8.2. *Flow from a source above the critical buoyancy flux*

The non-existence of a similarity solution for values of B greater than the critical value does not necessarily mean that there is no steady solution of the equation in this case. It seems highly likely that any such solutions must involve upstream propagation of the buoyant fluid. However, our scaling analysis of §4.1 indicates that the upstream intrusion cannot stabilize at a finite distance – but in order to conserve buoyancy, the upstream intrusion cannot extend to infinity for a finite source strength. Hence it would appear that only unsteady solutions are possible.

A numerical study by Valentine & Kao (1984) supports this conclusion. They calculated laminar flows in which a constant source of light fluid with Schmidt number 1 was switched on at the free surface of a channel flow with a Reynolds number 200. The volume flux of buoyant fluid was 20–25 % of the upstream volume flux in the channel. Valentine & Kao found that for $B > 1.38$ part of the inflow propagated upstream without reaching any limiting distance. They also computed a case with $B = 1$ in which it appeared that upstream propagation did not occur.

This critical value of B is considerably larger than we have found in the similarity solutions. The lack of quantitative agreement is probably due to the low Reynolds number and the large displacement thickness of the inflow relative to the channel depth, which must cause a significant pressure gradient tending to oppose the hydrostatic backflow.

5. Concluding remarks

I think that one can identify four main features of the mechanics of dense fluid emission into an ambient flow in two dimensions, as represented by these similarity solutions. While based on results on laminar flow, these features may also apply to turbulent flows such as heavy-gas emission over a horizontal surface, cooling-water discharges into flowing streams or rivers, and sea-water penetration into river mouths.

First, the extent of steady upstream spreading from the source of buoyant fluid is very sensitive to the shape of the oncoming velocity profile and also to external pressure gradients. The existence of two solutions with widely different properties for different lengthscales of intrusion into a uniform shear flow was caused by the different ways a pressure gradient induced by the oncoming flow affected the buoyancy-driven layer. The pressure gradient was caused by the displacement effect of the intrusion itself, but in general there might be other pressure gradients caused by the presence of an obstacle or the source of dense fluid downstream. Such externally induced pressure gradients are not normally considered in heavy-gas dispersion models at all. In turbulent flow, Jirka & Arita (1987) have demonstrated a sensitivity of the head shape of a density current or wedge to local velocity gradients, or the presence of small obstacles. It is not clear whether this is related to the mechanism described in this paper, for Jirka & Arita provide an explanation based on inviscid flow dynamics.

Secondly, the flow into a uniform velocity stream admits two possible states for the same buoyancy influx. I have termed these 'supercritical' when the plume is carried along at a fairly high speed and so remains shallow and develops a relatively small adverse pressure gradient, and 'subcritical' when the dense layer is deep and so moves rather slowly because of the large gradient of hydrostatic pressure, resulting in a low buoyancy flux. I am not sure whether this phenomenon is related

to the existence of critical flow in hydraulics, but one difference is that viscous drag from the free stream is a key factor in the mechanics here.

The third feature is linked to the second. There is a maximum buoyancy flux for which a steady plume exists. If a larger buoyancy flux is emitted then it appears that upstream propagation will occur. The upstream front will propagate indefinitely, not reaching any finite steady length.

The fourth feature is that contrary to what one might naively expect, negative buoyancy increases the depth of these plumes compared to passive dispersion. This is almost certainly a purely two-dimensional effect, as in three dimensions lateral spreading can occur making the plume thinner than its passive equivalent. In turbulent flow this conclusion might not apply because increasing stratification would tend to reduce mixing rates.

These features will require confirmation by experiment and by numerical solution of the partial differential equations.

This work was funded by the UK Health and Safety Executive.

REFERENCES

AFZAL, N. & HUSSAIN, T. 1984 Mixed convection over a horizontal plate. *Trans. ASME J. Heat Transfer* **106**, 240–241.

BRIGHTON, P. W. M. 1987 Similarity solutions for two-dimensional steady gravity currents. *Proc. IMA Conf. on Stably Stratified Flow and Dense Gas Dispersion, Chester, UK* (ed. J. S. Puttock). Oxford University Press.

GILL, W. N. & CASAL, E. DEL 1962 A theoretical investigation of natural convection effects in forced horizontal flows. *AIChE J.* **8**, 513–518.

HOOG, F. R. DE, LAMINGER, B. & WEISS, R. 1984 A numerical study of similarity solutions for combined forced and free convection. *Acta Mechanica* **51**, 139–149.

JIRKA, G. H. & ARITA, M. 1987 Density currents or density wedges: boundary-layer influence and control methods. *J. Fluid Mech.* **177**, 187–206.

RIDDELL, J. F. 1970 Densimetric exchange flow in rectangular channels. IV – the arrested saline wedge. *La Houille Blanche* **25**, 317–329.

SCHNEIDER, W. 1979 A similarity solution for combined forced and free convection flow over a horizontal plate. *Intl J. Heat Mass Transfer* **22**, 1401–1406.

SMITH, F. T. 1982 On the high Reynolds number theory of laminar flows. *IMAJ Appl. Maths* **28**, 207–281.

SMITH, F. T., BRIGHTON, P. W. M., JACKSON, P. S. & HUNT, J. C. R. 1981 On boundary-layer flow past two-dimensional obstacles. *J. Fluid Mech.* **113**, 123–152.

STEWARTSON, K. 1974 Multistructured boundary layers on flat plates and related bodies. *Adv. Appl. Mech.* **14**, 145–239.

VALENTINE, D. T. & KAO, T. W. 1984 Gravity current upstream of a buoyant influx in an open-channel flow: a numerical study. *J. Fluid Mech.* **140**, 303–327.